GFZ
Helmholtz-Zentrum
POTSDAM

Originally published as:

Ritter, M., Leever, K., Rosenau, M., Oncken, O. (2016): Scaling the Sand Box - Mechanical (Dis-) Similarities of Granular Materials and Brittle Rock. - *Journal of Geophysical Research*, *121*, 9, pp. 6863—6879.

DOI: http://doi.org/10.1002/2016JB012915

AGU PUBLICATIONS

JGR

Journal of Geophysical Research: Solid Earth

RESEARCH ARTICLE
10.1002/2016JB012915

Key Points:
- We measure transient strength of two granular analog materials at low normal stresses
- Strain weakening at normal load >1 kPa in granular materials is governed by loss of cohesion
- Quantitative comparison to natural values reveals scaling is only valid for crustal-scale models

Correspondence to:
M. C. Ritter,
malte.ritter@gfz-potsdam.de

Citation:
Ritter, M. C., K. Leever, M. Rosenau, and O. Oncken (2016), Scaling the sandbox—Mechanical (dis) similarities of granular materials and brittle rock, *J. Geophys. Res. Solid Earth*, *121*, 6863–6879, doi:10.1002/2016JB012915.

Received 11 FEB 2016
Accepted 25 AUG 2016
Accepted article online 29 AUG 2016
Published online 17 SEP 2016

©2016. American Geophysical Union. All Rights Reserved.

Scaling the sandbox—Mechanical (dis) similarities of granular materials and brittle rock

Malte C. Ritter[1], Karen Leever[1], Matthias Rosenau[1], and Onno Oncken[1]

[1] Helmholtz Center Potsdam German Research Center for Geosciences GFZ, Potsdam, Germany

Abstract Analog sandbox experiments are an important tool to understand brittle tectonic deformation. To date, most experiments are interpreted kinematically only. With the advent of reliable, small-scale force sensors, however, their dynamic evolution becomes available for analysis, offering new insights into the transient evolution of tectonic systems. Both rock and granular materials show an evolution of strain hardening and weakening during loading in the brittle-plastic regime, but so far, this similarity has only been appreciated qualitatively. As strain weakening is a vital parameter controlling fault reactivation and lifetime, it requires proper scaling. We therefore measured and analyzed two common granular analog model materials (quartz sand and glass microbeads) using ring-shear tests at a range of normal loads typical for analog experiments. We find two different modes of strain weakening as a function of normal load: Strain weakening at normal loads <1 kPa is due to partial loss of extrapolated cohesion, while at normal loads >1 kPa it is controlled by reduction of internal friction, which is consistent with previous measurements in this range. We show that this introduces a scale dependence into the scaling and restricts the possible use of the tested materials to crustal-scale models with a length scaling factor of $l(\frac{\text{model}}{\text{nature}}) \approx 2 \times 10^{-6}$. For these we quantitatively compare the model materials' transient strength evolution to that known from natural rock and the Earth's crust.

1. Introduction

Analog models are an important tool to understand tectonic deformation. In combination with modern imaging techniques they achieve a spatiotemporal resolution that neither natural data nor numerical models can provide [*Adam et al.*, 2005]. Most long-term models of the brittle upper crust use some kind of granular material ("sand") as a rock analog and study its kinematic behavior during compression [e.g., *Graveleau et al.*, 2012], extension [e. g, *Brun*, 1999], or strike-slip movement [e.g., *Dooley and Schreurs*, 2012]. Some recent experiments also include force measurements in an attempt to characterize the dynamics of the model [*Nieuwland et al.*, 2000; *Cubas et al.*, 2010, 2013; *Herbert et al.*, 2015].

For the observations from any model to be representative of a natural prototype it is crucial that the model be properly scaled to nature with respect to geometry, kinematics, and dynamics [*Hubbert*, 1937]. According to this author, three fundamental scaling factors need to be defined: one each for length, mass, and time, or, more commonly, length, density, and gravity:

$$l^* = \frac{l_{\text{model}}}{l_{\text{nature}}}, \rho^* = \frac{\rho_{\text{model}}}{\rho_{\text{nature}}}, g^* = \frac{g_{\text{model}}}{g_{\text{nature}}}. \quad (1)$$

All other necessary scaling factors can then be calculated from these. For tectonic models the most important other scaling factor would probably be that for stress, which can be derived from equation (1) as

$$\sigma^* = \rho^* g^* l^*. \quad (2)$$

If these scaling factors are taken care to be valid always and everywhere throughout the entire experiment, *Hubbert* [1937] states that scaling will be achieved. However, doing so for stress is not trivial, since it cannot be directly controlled but arises as a response of a material to the applied boundary conditions. Consequently, the material's response to boundary conditions, i.e., its rheology, must be the same as for the natural material [*Weijermars and Schmeling*, 1986], which for brittle prototypes means that the analog model material must be brittle as well and has to show the same transient strength evolution.

The common approach to achieve scaling is, apart from ensuring geometric similarity, to assume that both brittle rock and analog material behave according to a Mohr-Coulomb failure criterion:

$$\tau = \mu\sigma_n + C \tag{3}$$

where τ and σ_n are the shear stress and the normal stress on a failure plane, μ is the coefficient of internal friction, and C is the extrapolated cohesion. (In the following the term "cohesion" is always referring to this extrapolated cohesion unless stated otherwise. For a procedure to determine the true cohesion, see *Abdelmalak et al.* [2016]). Being small compared to $\mu\sigma_n$, C is often simply neglected for the purpose of scaling [*Davy and Cobbold*, 1988; *Buchanan and McClay*, 1991; *Tron and Brun*, 1991; *Duerto and McClay*, 2009]. This conveniently results in the single scaling condition that μ_{sand} and μ_{rock} be similar. μ_{sand} is commonly taken to be between 0.5 and 0.7 (based on, e.g., *Krantz* [1991]), and μ_{rock} is taken to be 0.6, based on Byerlee's law [*Byerlee*, 1978]. Consequently, models are assumed to be properly scaled.

Other modelers [*Gutscher et al.*, 1996; *Cobbold et al.*, 2001; *Galland et al.*, 2006; *Rosenau et al.*, 2009; *Burchardt and Walter*, 2010; *Galland et al.*, 2014; *Abdelmalak et al.*, 2016] do scale C, using the geometry of their setups and the density of their model materials. They all come to the conclusion that their models are properly scaled for C_{nature} ranging somewhere from 10^5 Pa to 10^7 Pa, depending on their materials and modeled settings. According to these authors, this range of values represents the natural materials in their respective cases quite well.

The major problem of this common approach is that the Mohr-Coulomb failure criterion does not account for any transient postfailure behavior of a material. This is particularly unfortunate since the postfailure phase is the one during which most significant tectonic evolution takes place. It is characterized by a loss of strength with progressive deformation known as "strain weakening," in both rock [*Bieniawski et al.*, 1969] and sand [*Kolymbas and Wu*, 1990; *Desrues and Viggiani*, 2004]. Strain weakening is assumed to be closely linked to strain localization and fault formation. Accordingly, it is an additional material property that should be properly scaled in tectonic models. *Lohrmann et al.* [2003] were the first to recognize this and to qualitatively compare the shapes of failure curves of natural rock and quartz sand. From measurements in a ring-shear tester they defined three Mohr-Coulomb-type failure envelopes for quartz sand, corresponding to the different stages during deformation: peak strength, stable strength, and reactivation strength (Figure 1). They did not, however, quantitatively compare these strength values to those of natural materials. *Panien et al.* [2006] determined the same mechanical parameters for several other analog materials but did not relate them to natural data either. Therefore, a quantitative comparison of the transient mechanical behavior of granular analog materials to nature is still missing to date, and its scaling remains to be determined.

Another problem of the above scaling approach, although not inherent to it, is the mechanical testing of the analog material itself. It is usually carried out at normal loads of a few kPa [*Krantz*, 1991; *Lohrmann et al.*, 2003; *Panien et al.*, 2006] to a few hundred kPa [*Kolymbas and Wu*, 1990]. This yields linear failure envelopes for peak and stable strength that differ mainly by slope, i.e., friction coefficient. However, the overburden load at the bottom of a 5 cm thick layer of sand, which is a typical height of an analog model, is $\rho gh \approx 1700\,\mathrm{kgm^{-3}} \times 9.81\,\mathrm{ms^{-2}} \times 0.05\,\mathrm{m} = 834\,\mathrm{Pa}$ and thus below the range of the test data. It is therefore unclear whether the data obtained in these studies are representative for the material's behavior under model conditions.

Schellart [2000] tested different granular materials at very low normal loads (50 Pa to 900 Pa) and found that for this range the failure envelope of the peak strength shows a convex shape. He attributed the observed deviation from the linear Mohr-Coulomb envelope to a reduction of apparent cohesion. Stable strength and weakening were not measured in this study, owing to the nature of the experimental device used.

The data in *Schellart* [2000], as well as in *Krantz* [1991] and most of *Lohrmann et al.* [2003], have been obtained using a so-called "Hubbert-type" shear box. This device consists of two cylinders of equal diameter that are placed above each other with a thin gap in between. They are filled with the tested material; then the upper one is moved laterally, thereby shearing the material at the transition between the cylinders. Its strength can be calculated from the contact area between the two cylinders and the force required to move the upper cylinder. There are some issues with this approach though, the main one being that the shear zone does not necessarily remain between the cylinders as a plane feature. For small thicknesses of the layer above the shear zone ($h < \frac{r}{3}$, where r is the radius of the cylinder) it may bend upward [*Schellart*, 2000] or even evolve into a thrust cross-cutting the sample. Obviously, this would bias the results. *Schellart* [2000] provides a detailed discussion of possible sources of error related to the Hubbert-type apparatus.

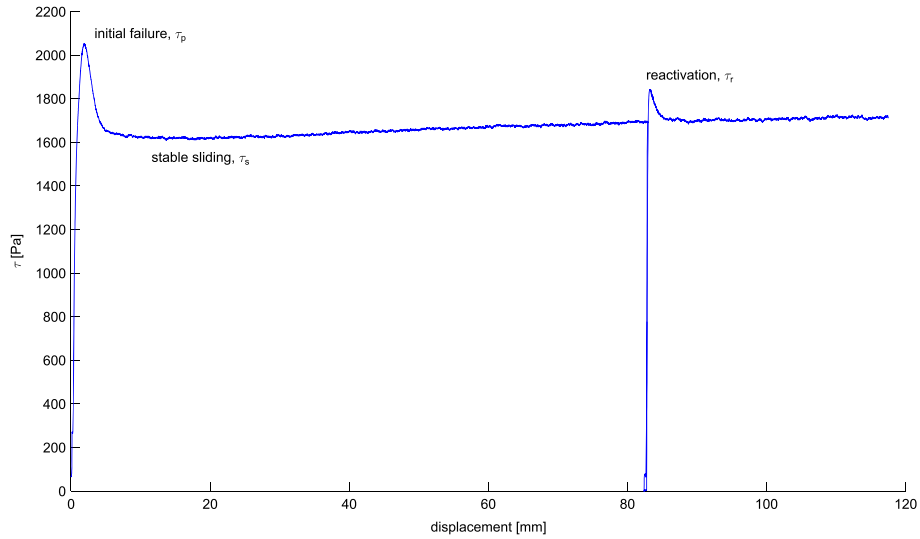

Figure 1. Characteristic shear stress—displacement curve (shear curve) for quartz sand at $\sigma_n = 3$ kPa, obtained using the ring-shear tester (RST). Strain localization into a discrete shear zone is associated with a peak in the diagram due to hardening and subsequent weakening (initial failure, τ_p). Smaller hardening—weakening precedes reactivation (τ_r). The horizontal part of the curve is associated with stable sliding on the shear zone (τ_s). The slight increase is due to the lid of the shear cell burrowing slowly into the material.

In this study we aim to address the issues mentioned above: We first create a set of mechanical data for two common analog materials, that covers the entire range of relevant normal loads and is large enough to account for statistical variability. We do this through measurements with a ring-shear tester [*Schulze*, 1994] that due to its design avoids the problems of the Hubbert-type apparatus. We then quantitatively compare this data set to natural data to assess the analog materials' suitability for tectonic modeling, taking into account the transient material behavior during failure.

2. Materials and Methods

We use two granular materials that are both commonly applied in analog modeling: quartz sand and glass beads. The quartz sand (type G23T) is a moderately sorted, medium-grained fluvial sand, with rounded grains and a mean grain size of 300 μm. It is the standard sand used for analog modeling at GFZ Potsdam and represents a rather coarse variant of sands used by the analog modeling community. However, friction and cohesion values are similar to sands from other laboratories [*Klinkmüller et al.*, 2016a, Figures 3a and 3b]. The glass beads are an artificial product. They are nearly perfectly rounded and very well sorted, with a grain size distribution ranging from 100 μm to 200 μm and a mean grain size of 175 μm. They represent rather fine-grained and low friction and cohesion material compared to commonly used sands [*Klinkmüller et al.*, 2016a Figures 3a and 3b].

Measurements are carried out in the ring-shear tester RST-01.pc [*Schulze*, 1994] which has also been used by *Lohrmann et al.* [2003] and *Panien et al.* [2006]. It consists of an annular shear cell containing the sample (inner radius: 5 cm, outer radius: 10 cm, and height: 4 cm), and a lid that is pressed onto the sample at a preset normal load which is kept constant throughout an experiment (Figure 2). The shear cell is rotated, while the lid is kept in place. Closely spaced radial blades pointing vertically downward from the lid (distance: 17.9 mm at inner edge, 30.2 mm at outer edge; height: 5 mm, and thickness: 0.9 mm) ensure that it is mechanically coupled with the sample, such that all relative displacement between lid and shear cell must be taken up by the sample. Sensors at the lid record the torque transferred from the shear cell via the sample to the lid, as well as the lid's vertical movement which is equivalent to the sample dilation. Knowing the geometry of the device, one can transform the torque measurements into shear stress (τ) and the rotation into displacement and plot those as shear curves (Figure 1). This device has been benchmarked using a certified standard bulk material (limestone powder CRM-116), and the results have been found to be consistent with those of a Jenike shear cell [*Schulze*, 1994]. The Jenike shear cell is mechanically equivalent to the Hubbert-type shear box that is commonly applied in the analogue modeling community.

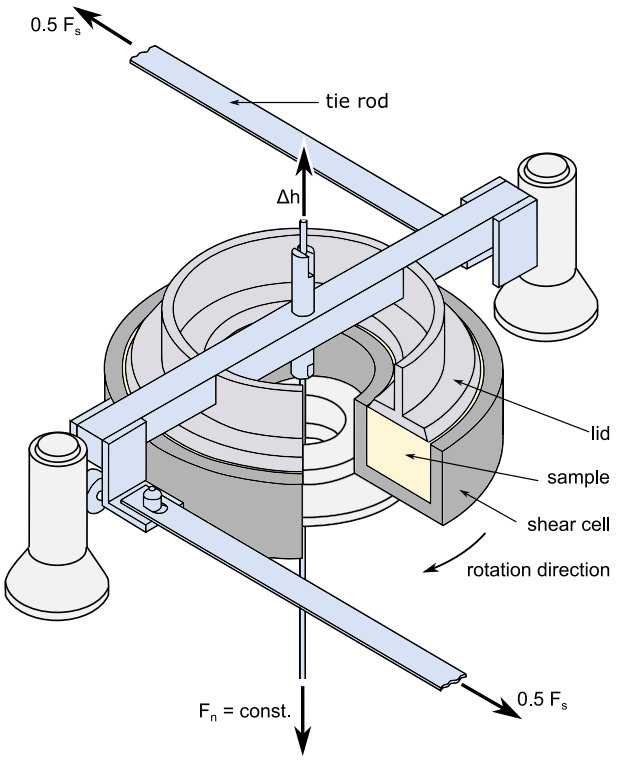

Figure 2. Sketch of the ring-shear tester, modified from *Panien et al.* [2006]. The material is sifted into the shear cell, then the lid is placed on top of it, and a constant normal load F_n is applied through a weight. The cell is then rotated, while the lid is kept in place by tie rods. Due to this differential movement between shear cell and lid, a shear zone forms within a sample. Force sensors register the shearing force F_s, which can be transformed into shear stress within the sample using the known geometry of the device. Dilation of the sample is measured as the vertical movement Δh of the lid.

At the onset of deformation shear stress first increases quickly to a maximum τ_p and then drops to a stable value τ_s, which it retains for the rest of the deformation. When deformation is stopped, the sample unloaded and subsequently deformation is resumed, another stress peak occurs which is called reactivation strength τ_r. It is usually somewhat smaller than τ_p. Detailed inspection of Figure 1 reveals that this stable value is actually slightly increasing. This is an artifact of the setup and due to the fact that the lid of the shear cell slowly burrows into the material upon continued shearing, thereby increasing the friction at its side walls. It causes a tendency to overestimate τ_r. For exact an determination of the reactivation stress this should be corrected for using the measurement of the vertical displacement of the lid. The three stress values were automatically picked from the shear curves and form the base of the following analysis, in which we will concentrate on τ_p and τ_s and report the values of τ_r merely for the sake of completeness. The automatic picking algorithm finds the two maxima of the shear curves, which are τ_p and τ_r, and then finds the minimum in between the two peaks, which is τ_s. The unloading phase is detected via the rotation velocity and masked out prior to determining the peaks.

Samples were sifted into the shear cell to achieve high compaction [*Krantz*, 1991], and measurements were carried out for different normal loads ranging from 125 Pa to 4000 Pa, repeating them 8 to 10 times per normal load. Samples measured at normal loads below 500 Pa were preloaded at 500 Pa to make sure that the blades were fully immersed in the sand, and the lid was in close contact with the sample. Preliminary tests at a normal load of 300 Pa have shown that this does not affect the strength.

3. Results

In total 102 measurements were carried out for quartz sand and 83 for glass beads. The complete shear curves for all of them are available in the supplementary data publication of *Ritter et al.* [2016]. In the following we use only τ_p, τ_s, and τ_r derived from the shear curves. We divide them in two data sets, one containing all measurements for quartz sand and one for those of glass beads. Both data sets show an approximately linear increase of all three values with σ_n, and neither shows the convex shape of the failure envelope observed by *Schellart* [2000] for low σ_n (Figures 3a and 3b). This is consistent with a Mohr-Coulomb failure criterion. The strength of the quartz sand is generally higher than that of the glass beads. In order to quantify the strength drop from τ_p to τ_s, we define the relative weakening $\Delta\tau$ as

$$\Delta\tau = 1 - \frac{\tau_s}{\tau_p} = 1 - \frac{\mu_s\sigma_n + C_s}{\mu_p\sigma_n + C_p}. \quad (4)$$

This value will be between zero (no weakening) and one (no residual strength). For high normal loads it will be dominated by μ and converge toward $1 - \frac{\mu_s}{\mu_p}$, whereas for normal loads approaching zero it will be dominated by C and converge toward $1 - \frac{C_s}{C_p}$. Figures 3c and 3d shows $\Delta\tau$ for both data sets. In either case $\Delta\tau$ is highest

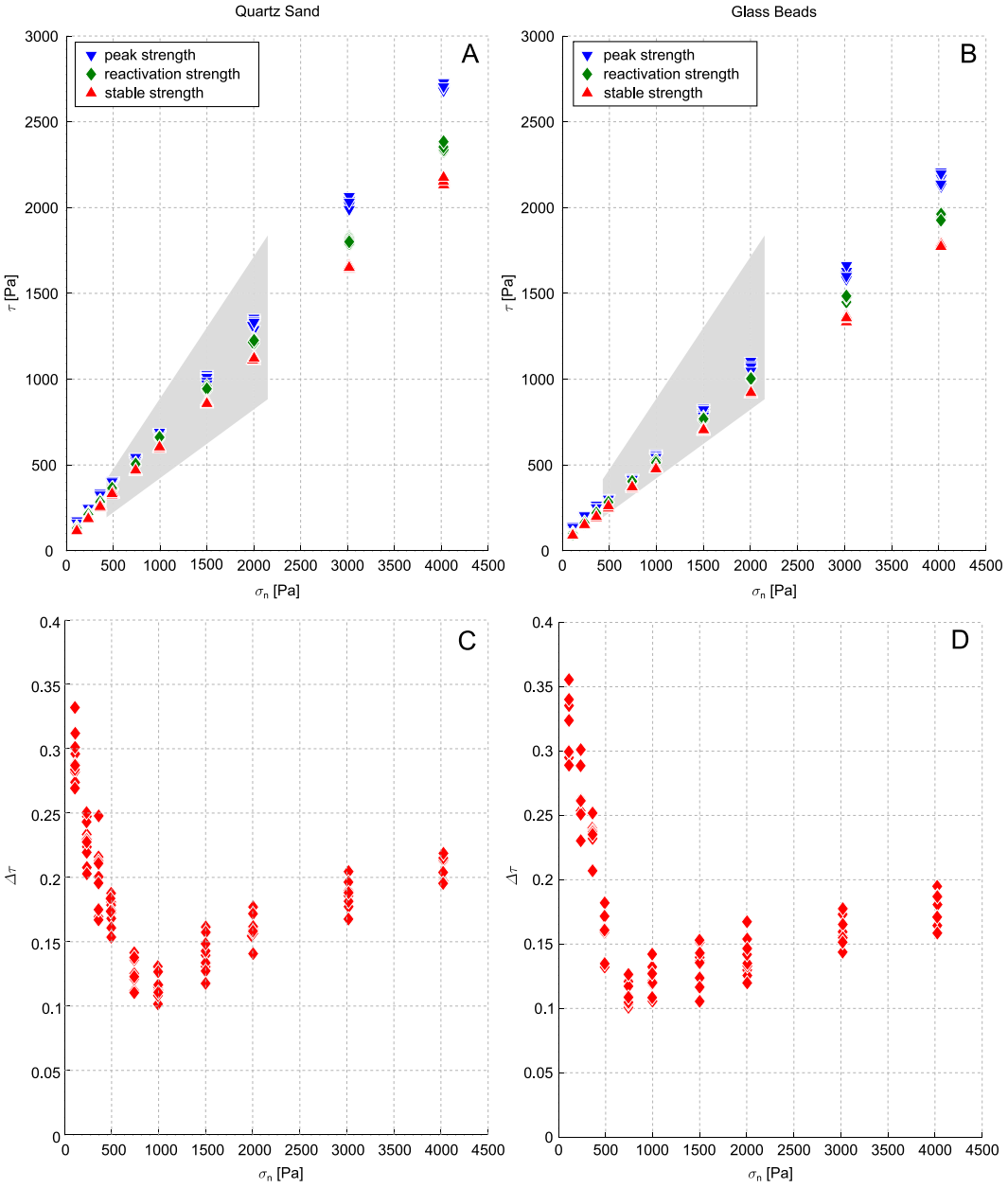

Figure 3. Shear strength as function of normal load of (a) quartz sand and (b) glass beads, measured with the ring-shear tester (the raw data are published in *Ritter et al.* [2016]). The data show an approximately linear increase with normal load, which is consistent with the assumption of a Mohr-Coulomb failure criterion. The strength of quartz sand is generally higher than that of glass beads, and the peak strength of each material shows a higher slope than the respective stable and reactivation strengths. The gray patch shows the range of other common analog model materials as determined by *Klinkmüller et al.* [2016b]. Relative weakening $\Delta\tau = 1 - \frac{\tau_s}{\tau_p}$ as function of normal load of (c) quartz sand and (d) glass beads. Neither of the data sets show the monotonic behavior expected from the definition of $\Delta\tau$ and linear failure envelopes.

(about 0.35) for low normal loads, decreases toward a minimum of about 0.1 at $\sigma_n \approx 1$ kPa and then reaches a stable value of roughly 0.2 at high normal loads. This shape is inconsistent with the assumption of linear τ and positive σ_n, for which, according to the definition in equation (4), $\Delta\tau$ should be monotonic: If $\tau_{s,p}$ are simple linear functions (equation (3)), they are differentiable. Thus, $\Delta\tau$ is differentiable as well. It has a pole for $\tau_p = 0$ and no other extremum. This can be verified by setting

$$\frac{\partial \Delta\tau}{\partial \sigma_n} = \frac{\mu_p C_s - \mu_s C_p}{\tau_p^2} \equiv 0 \tag{5}$$

Table 1. Mechanical Properties of the Investigated Materials, as Determined by Linear Least Squares Fitting of τ_p, τ_r, and τ_s at Different Normal Loads[a]

	μ_p	C_p (Pa)	μ_r	C_r (Pa)	μ_s	C_s (Pa)
Quartz sand, $\sigma_n \geq 1$ kPa	0.672(5)	0(13)	0.562(4)	101(9)	0.524(3)	91(6)
Quartz sand, $\sigma_n \leq 1$ kPa	0.576(7)	110(4)	0.591(4)	70(2)	0.546(3)	60(2)
Glass beads, $\sigma_n \geq 1$ kPa	0.536(7)	0(17)	0.471(3)	58(6)	0.429(2)	57(4)
Glass beads, $\sigma_n \leq 1$ kPa	0.459(9)	85(5)	0.478(3)	47(2)	0.443(4)	40(3)

[a]The numbers in parentheses are the numerical values of measurement uncertainty, calculated as twice the standard deviation of the respective fit parameter, and referred to the corresponding last digits of the result.

which yields no solution for σ_n, except for the case of $\mu_p C_s - \mu_s C_p = 0$, in which it becomes true for any σ_n. For physical reasons $\tau_p > 0$ for $\sigma_n \in (0, \infty)$, and thus, $\Delta\tau$ must be monotonic in this interval.

We therefore divide both data sets at their respective minimum of $\Delta\tau$ in two subsets, such that each subset individually satisfies this criterion. The "low-load" subsets comprise all measurements of the respective material for which $\sigma_n \leq 1$ kPa and the "high-load" subsets all those for which $\sigma_n \geq 1$ kPa. For each subset a linear least squares algorithm is applied to find the best fitting Mohr-Coulomb failure envelope (equation (3)). The fitting parameters μ and C for each subset are listed in Table 1.

The high-load subsets (Figures 4a and 4b) show similar characteristics as observed in previous studies [*Mandl et al.*, 1977; *Lohrmann et al.*, 2003; *Panien et al.*, 2006]: The failure envelopes for peak, stable and reactivation strength diverge, with friction coefficients of $\mu_p \approx 0.7$ and $\mu_s \approx 0.5$ for quartz sand, and $\mu_p \approx 0.5$ and $\mu_s \approx 0.4$ for glass beads. $\Delta\tau$ is similar for both materials and increases from 0.1 to 0.2 over the range of the subset (Figures 4c and 4d). This increase is mainly due to $C_p \ll C_s$ for both materials, which makes the derivative in equation (5) positive.

This is remarkably different for the low-load subsets (Figures 5a and 5b). Here peak friction coefficients are significantly lower than in the high-load subset, particularly for the quartz sand. At the same time, friction coefficients for reactivation and stable strength remain approximately constant. This results in the failure envelopes of peak and stable strength being almost parallel. Consequently, the weakening is mainly controlled by cohesion, which shows an offset of about 50 Pa between peak and stable strength for both materials. According to equation (5), this results in decreasing $\Delta\tau$. It starts around 0.3 to 0.35 for $\sigma_n = 125$ Pa and decreases to 0.1 to 0.15 for $\sigma_n = 1000$ Pa (Figures 5c and 5d). It is slightly higher in glass beads than in quartz sand owing to the quartz sand's higher peak strength.

4. Discussion

4.1. Validation of Measurements

Deformation in the ring-shear tester used in this study is, in general, similar to that in the Hubbert-type shear box. As a main difference there is not one single back wall at which failure initiates—as in the Hubbert-type apparatus—but several blades at each of which a small shear zone initiates and propagates to link up with the next shear zone at the next blade. Conceptually, the ring-shear tester can be regarded as a series of small-scale Hubbert-type shear boxes that are each bounded by two adjacent blades. Therefore, the measured shear stress is averaged over several developing shear zones, which makes the results more stable. The mechanical processes within the sample, however, are the same.

The data set we have obtained in our measurements spans a wider range of normal load conditions than any previous study: *Lohrmann et al.* [2003] measured quartz sand similar to ours (their sands "SIC2" and "SHC") at normal load conditions corresponding to our high-load range. Friction coefficients and cohesion they derive for peak and reactivation show the same trend and very similar values as ours. Since they used a Hubbert-type shear box, they could not measure weakening as we define it. *Panien et al.* [2006] carried out ring-shear measurements on several granular materials and determined also the relative weakening. In the high-load range, in which they measured, they find the same slightly increasing trend of the relative weakening as we do (Figures 4c and 4d); their Figure 3). *Klinkmüller et al.* [2016a] measured various materials at normal loads ranging from 430 Pa to 2150 Pa, among them also those used in this study. They used the same ring-shear tester as we did and found friction coefficients that match those of our high-load subset quite well. Their range of normal loads overlaps slightly with our low-load subset; however, they do not report the increase of weakening

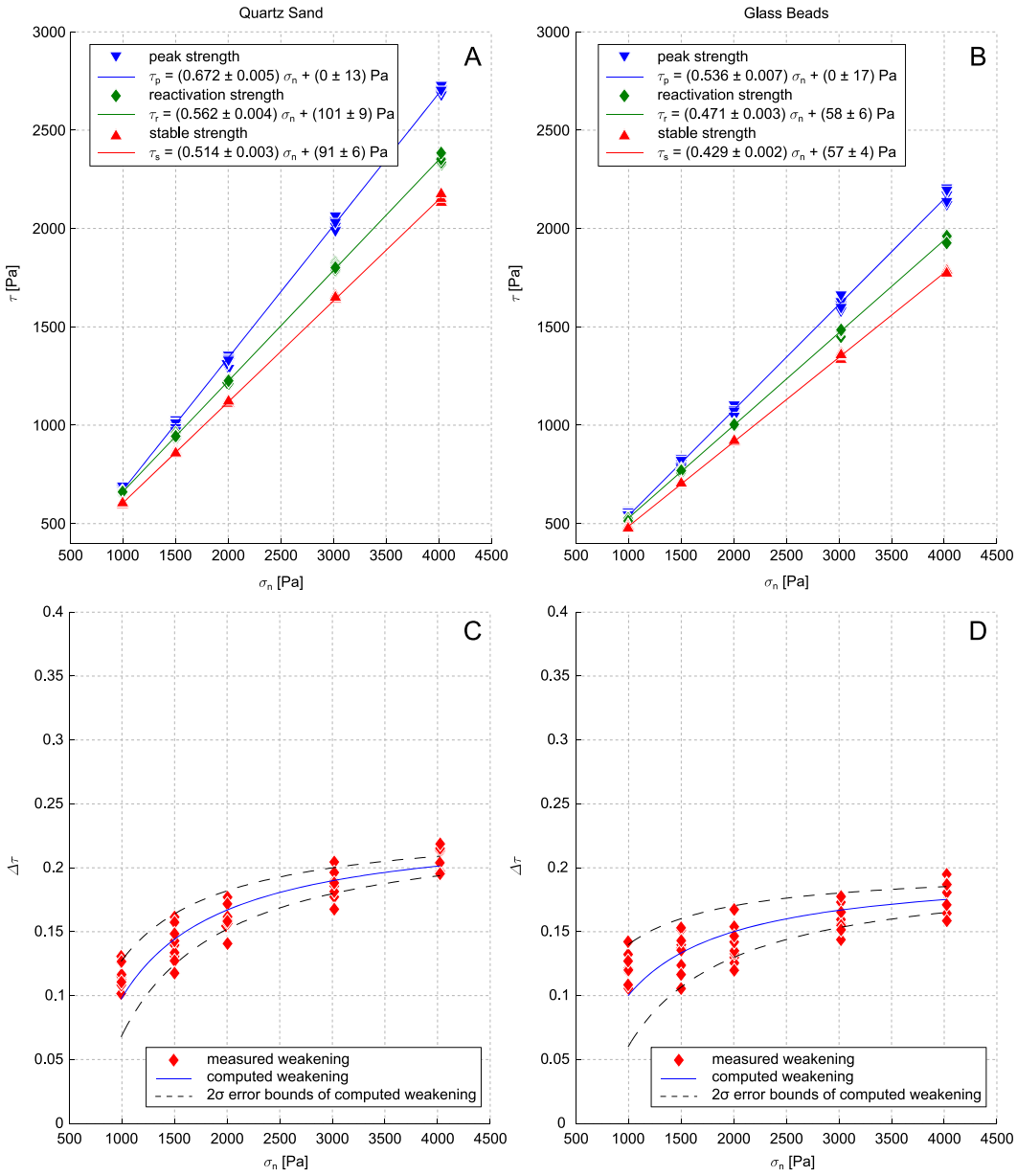

Figure 4. Shear strength as a function of normal load for the high-load subset of (a) quartz sand and (b) glass beads. The lines represent Mohr-Coulomb failure envelopes fitted by means of a linear least squares algorithm. The three failure envelopes for each material diverge, indicating a weakening mechanism controlled by reduction of internal friction. Relative weakening $\Delta\tau = 1 - \frac{\tau_s}{\tau_p}$ as function of normal load for (c) quartz sand and (d) glass beads in the high-load subset. For both materials is $\Delta\tau$ is slightly increasing with σ_n. The computed weakening is the result of inserting the equations of the fitted failure envelopes into equation (4).

we observe for low normal loads. The good agreement of the parameters measured in those previous studies with our measurements validates our results for the high-load subset. For the low load subset validation is not possible because of a lack of data in this range.

The only measurements carried out at low normal loads that we are aware of are those of *Schellart* [2000] and *van Mechelen* [2004]. The latter study measured internal friction and cohesion of different sands and glass beads (wet and dry) at normal loads between 200 Pa to 1000 Pa. However, the results are not directly comparable to ours since the materials used are different, and the study of *van Mechelen* [2004] concentrates on low normal loads and could thus not have found the transition to the high-load regime.

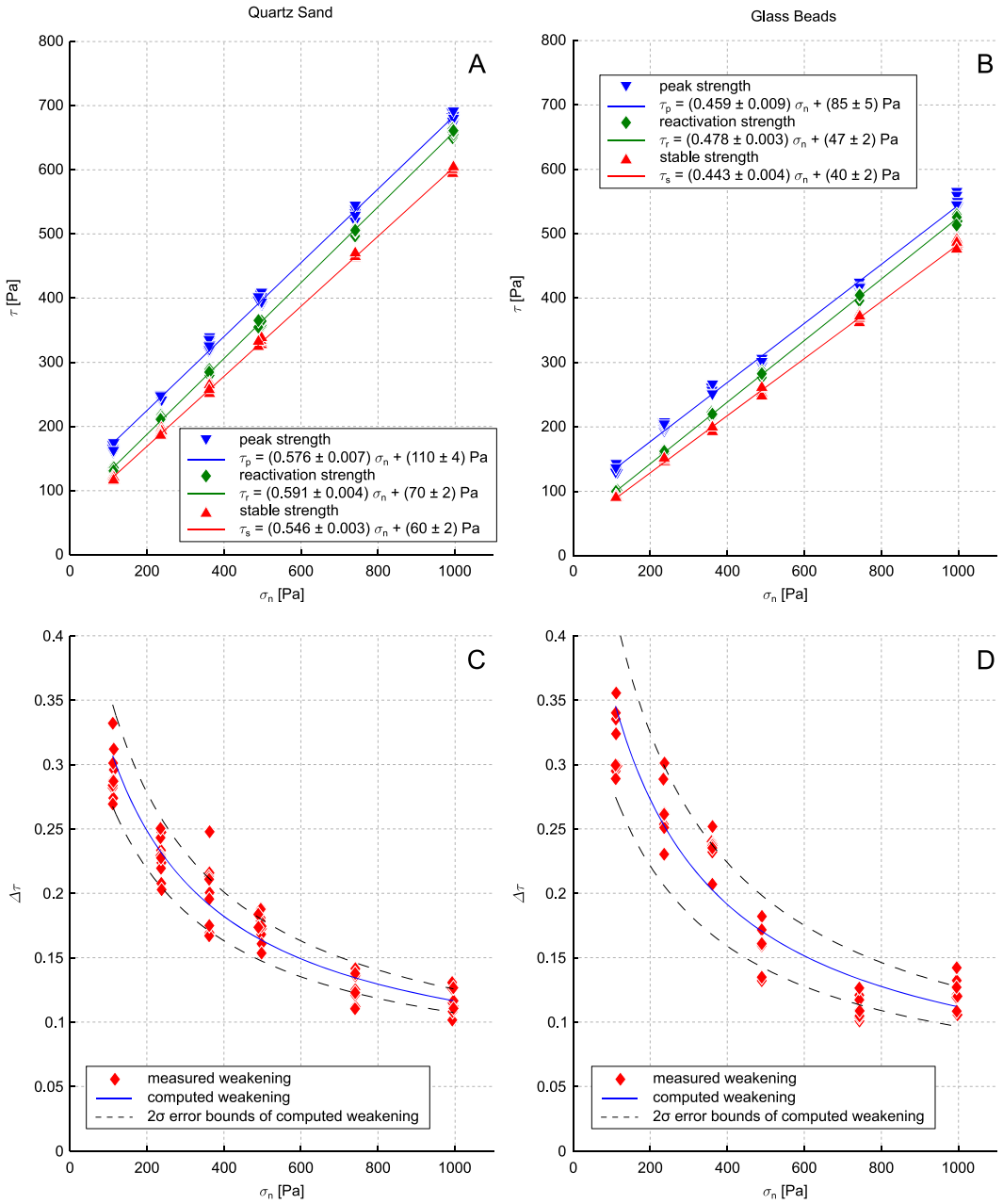

Figure 5. Shear strength as a function of normal load for the low-load subset of (a) quartz sand and (b) glass beads. The lines represent Mohr-Coulomb failure envelopes fitted by means of a linear least squares algorithm. Compared to the high-load subset, peak friction is much lower in this subset, especially for quartz sand. This results in the failure envelopes of peak and stable strength being almost parallel, which indicates a weakening mechanism controlled by reduction of cohesion rather than internal friction. Relative weakening $\Delta\tau = 1 - \frac{\tau_s}{\tau_p}$ as function of normal load for (c) quartz sand and (d) glass beads in the low-load subset. For both materials is $\Delta\tau$ is decreasing with σ_n. Values for glass beads are slightly higher than for quartz sand, due to the glass beads' lower peak strength.

Schellart [2000] reports peak strengths of several granular materials for normal loads matching our low-load subset and below, which he measured in a Hubbert-type apparatus. He observed a convex shape of the failure envelope for very low normal loads below 300 Pa, which is not visible in our data. It is possible, however, that this convex shape does also exist in our materials but only occurs for lower normal loads than we were able to measure.

4.2. Consequences for Scaling

In the common scaling approach in tectonic modelling—as described above—the influence of cohesion C is often neglected. Strength in that case only depends on normal load through a constant factor, the friction coefficient. Since strength and normal load both scale as stresses, it is then assumed that strength is properly scaled as long as friction is the same and normal load is scaled, independently of the actual dimensions of the model. Granular materials have been used accordingly to model processes at scales ranging from basin- or accretionary wedge-scale [*McClay*, 1990], over crustal- or orogenic wedge-scale [*Leever et al.*, 2011; *Graveleau et al.*, 2012] up to even lithospheric scale [*Davy and Cobbold*, 1988; *Luth et al.*, 2013]. Our results, on the contrary, show that for the dimensions of typical analog models the weakening of granular materials is controlled by cohesion. As a consequence, cohesion should be taken into account for the scaling of processes in which weakening is important. This renders the initial assumption invalid and introduces a scale dependence of the material strength which is likely to restrict the possible uses of analog materials to only some of the above processes. Other models already include cohesion in the scaling, [e.g. *Galland et al.*, 2006; *Holohan et al.*, 2013; *Abdelmalak et al.*, 2016]. However, in these studies weakening is usually not considered.

In order to derive dynamic scaling of an analog material, one has to determine the strength of the natural prototype first. *Lohrmann et al.* [2003] and *Panien et al.* [2006] used laboratory-derived rock failure strengths for a qualitative comparison to analog material strengths, suggesting different analog materials to model different rock types. This implies the assumption that the strength of small rock samples under laboratory conditions correctly reflects rock strength on a larger, natural scale, and although it is rarely stated explicitly, this assumption can be found quite often in the analog modeling literature.

Studies on crustal rheology, on the other hand, usually assume the brittle part of the crust to be best described by Byerlee's law [*Byerlee*, 1978; *Brace and Kohlstedt*, 1980; *Bürgmann and Dresen*, 2008], which is an empirical law that describes the onset of sliding in a precut, laboratory-scale rock sample under shear stress as a function of normal load. This assumption is based on hydrofracturing experiments in deep boreholes, which measure crustal fracture strength on a kilometer scale and consistently find friction coefficients between 0.6 and 1 in most locations [*Brudy et al.*, 1997; *Townend and Zoback*, 2000], which are the same values as given by Byerlee's law. It is commonly explained by fractures crosscutting the upper crust in all directions, such that its strength will be determined by the reactivation of these fractures and not the fracturing of intact rock, if a large enough volume of rock is considered [*Brace and Kohlstedt*, 1980].

Depending on the situation and processes modeled, either of these two assumptions might be better suited. In the following, we analyze both and determine to which extent and at what scales our model materials correctly mimic the assumed natural behavior for each. In either case we define the natural processes to be represented by the analog material's peak and stable strength and then try to determine suitable scaling parameters by trial-and-error and simple comparisons. Prior to this, we analyze the influence of the weakening mode (by reduction of cohesion or friction).

4.2.1. Influence of Weakening

Strain weakening is crucial to maintain activity of a shear zone and to facilitate its reactivation: With progressing deformation a shear zone often rotates away from the initial, ideal orientation. The weakening determines how long it can still remain active, i.e., how much it can rotate until formation of a new shear zone will be mechanically more favorable than continuing activity on the existing one ("maximum rotation angle"). This can be illustrated in a Mohr-Coulomb diagram [*Scholz*, 2002]. Figure 6a shows this for a hypothetical material that weakens by reduction of friction, as commonly assumed for analog materials. In this case the absolute weakening increases with normal load, but the relative weakening remains constant. The slopes of the failure envelopes (μ) depicted are the same as we measured for quartz sand at high normal loads, but cohesion (C) is set to zero for simplicity. As can be seen from the diagram, the maximum rotation angle is independent of normal stress and always −18° to 13° around the dynamically ideal orientation (where the negative sign refers to clockwise rotation in the Mohr-Coulomb diagram).

Figure 6b shows the same Mohr-Circle construction for a material similar to quartz sand in the low-load regime, with $\mu = 0.57$ and cohesion $C_p = 110$ Pa and $C_s = 60$ Pa for peak and stable strength, respectively. In this case, which is representative for the situation in sandbox models, absolute weakening is constant, but relative weakening decreases with increasing normal load. Consequently, the range of orientations facilitating continued shear zone activity decreases with increasing normal load. The two Mohr circles shown represent the overburden stress at the base of a 1 cm thick and a 4 cm thick layer of sand. For an overburden of 1 cm

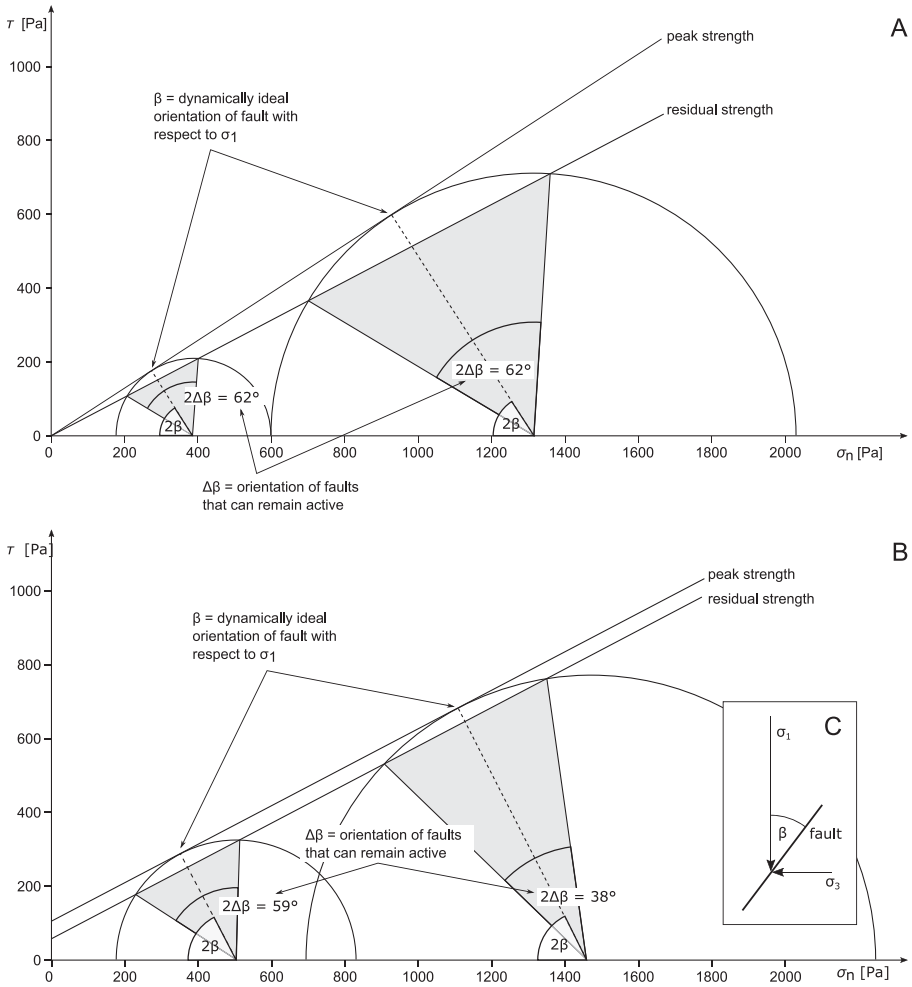

Figure 6. Mohr-Circle constructions showing the influence of weakening on shear zone activity for (a) a material that weakens by reduction of friction ($\mu_p = 0.67$, $\mu_s = 0.52$, $C = 0$; similar to quartz sand under high-load conditions) and (b) a material that weakens by partial loss of cohesion ($\mu_p = \mu_s = 0.57$, $C_p = 110$ Pa, $C_s = 60$ Pa; similar to quartz sand under loading conditions relevant for analog models). In Figure 6a the relative weakening is constant which results in a constant range of fault orientations, $\Delta\beta$, that can remain active (maximum rotation angle). In Figure 6b relative weakening decreases with increasing normal load and so does $\Delta\theta$. The Mohr-Circles show the state of stress at the base of a 1 cm and a 4 cm thick layer of sand, respectively. Both cases are idealized to emphasize the principal behavior. (c) The definition of β. Please note that angles are doubled in Mohr space.

sand, shear zones may rotate ±15° and remain active. For an overburden of 4 cm only ±10° of rotation are possible. These angles can be geometrically related to the distance between the failure envelopes at the point of failure and thus to the relative weakening. A similar construction could be carried out for the reactivation strength.

The cases described above are idealized, since for the real sand cohesion in the high-load regime is not exactly zero, and friction coefficients in the low-load regime are not exactly the same. Nevertheless, the general trend remains and shows a minimum range of possible shear zone rotation for continued activity at layer thicknesses of around 5 cm. This variable range has implications for any model in which strain is accommodated on networks of faults, in which partitioning of slip on individual structures is controlled by their potential for continued activity or reactivation. A narrower range of allowed shear zone rotation (i.e., smaller relative weakening) results in a shorter lifetime of shear zones and thus in more shear zones to be formed during a certain amount of time. Therefore, special care must be taken to properly scale the relative weakening and thereby the range of shear zone activity.

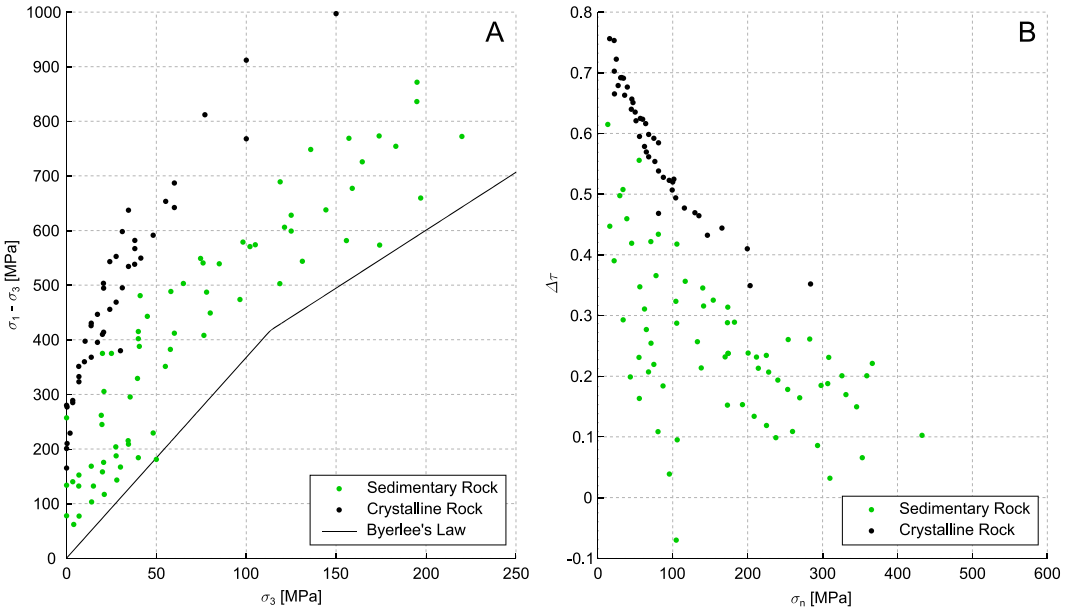

Figure 7. (a) Stress at failure for several types of rock in drained biaxial testing at different confining pressures. The solid line marks Byerlee's empirical law [*Byerlee*, 1978] for initiation of sliding on precut (failed) rock. (b) Relative weakening $\Delta\tau$ of rock, assuming Byerlee's law [*Byerlee*, 1978] as the representation of the weakened shear stress τ_s. Note that this is only an upper bound approximation for τ_s, real $\Delta\tau$ will in fact be larger. All data are rotated into (σ_n, τ)—space using the friction angles ϕ given in Table 2. All data are compiled from literature.

4.2.2. Comparison to Intact Rock

The rock failure data used to compare our measured data to were compiled from literature. *Al-Ajmi and Zimmerman* [2005] provided data in numerical form, all other data have been digitized from published plots. In *Byerlee* [1975] they were given in terms of stresses at failure, whereas *Byerlee* [1968], *Bieniawski et al.* [1969], *Crouch* [1970, 1971], and *Wawersik and Fairhurst* [1970] provided characteristic failure curves from which the stresses at failure were picked by hand. All data were given in terms of principal stresses σ_1 and σ_3. Figure 7a shows the failure strength as differential stress $(\sigma_1 - \sigma_3)$ versus confining pressure (σ_3). This figure shows a reasonably good linear correlation for the individual rock types. Therefore, a linear Mohr-Coulomb failure criterion can be fitted to each rock data set. In (σ_1, σ_3)—space this takes the form [*Jaeger et al.*, 2007]:

$$\sigma_1 = q\sigma_3 + C_0 \tag{6}$$

where the parameters q and C_0 can be related to the angle of internal friction ϕ and the cohesion C as

$$q = \frac{1 + \sin\phi}{1 - \sin\phi} \tag{7}$$

$$C_0 = 2C\frac{\cos\phi}{1 - \sin\phi}. \tag{8}$$

Using these relations, the angle β between σ_1 and the failure plane, i.e., τ, can be calculated [*Jaeger et al.*, 2007]:

$$\beta = 45° - \frac{1}{2}\phi. \tag{9}$$

By constructing the principal stress tensor and rotating it by β, each data point can individually be transformed from (σ_1, σ_3)—space to (τ, σ_n)—space in order to use the same coordinate system for all data, rock, and sand. The rock fitting parameters for either coordinate system can be found in Table 2.

Because of technical issues related to the high stiffness of rock, which is similar to that of common rock-testing machines [*Cook*, 1965; *Wawersik and Fairhurst*, 1970], practically, no complete stress-strain curves including the stable sliding regime are available for rock. Instead, we use Byerlee's empirical law as an estimate for the

Table 2. Mechanical Fit Parameters (Peak Strength) of the Different Rock Types Used in This Study

Rock Type	q	C_0 (MPa)	ϕ (deg)	μ	C (MPa)
Oak Hall limestone[a]	2.63	417	26.7	0.503	128
Marble[b]	2.98	136	29.8	0.574	39
Norite[c]	7.78	279	50.6	1.216	50
Norite[d]	11.85	278	57.6	1.575	40
Quartzite[e]	12.69	246	58.6	1.641	34
Weber sandstone A[f]	3.23	227	31.8	0.620	63
Weber sandstone B[f]	4.09	217	37.4	0.764	54
Weber sandstone C[f]	4.09	285	37.4	0.764	70
Marble[g]	4.23	52.7	38.1	0.785	13
Dunham dolomite[g]	3.66	299	34.8	0.696	78
KTB amphibolite[g]	6.44	220	47.0	1.072	43
Shirahama sandstone[g]	2.31	124	23.4	0.432	41
Solnhofen limestone[g]	2.09	358	20.7	0.378	124
Westerly granite[g]	8.17	250	51.4	1.254	44

[a] *Byerlee* [1968].
[b] *Wawersik and Fairhurst* [1970].
[c] *Crouch* [1971].
[d] *Bieniawski et al.* [1969].
[e] *Crouch* [1970].
[f] *Byerlee* [1975].
[g] *Al-Ajmi and Zimmerman* [2005].

stable strength. It states that peak shear stress for sliding on a preexisting fracture plane is independent of rock type and follows [*Byerlee*, 1978]

$$\begin{aligned} \tau &= 0.85\sigma_n \qquad \text{for} \sigma_n \leq 200\ \text{MPa and} \\ \tau &= 0.60\sigma_n + 50\ \text{MPa} \qquad \text{for} \sigma_n \geq 200\ \text{MPa}. \end{aligned} \tag{10}$$

This corresponds to the reactivation stress τ_r as measured in the ring-shear tester and can serve as an upper bound for τ_s only; however, it is the best approximation available. Byerlee's law is shown in Figure 7a as a black line. Figure 7b shows the relative weakening $\Delta\tau$ for the different rock types assuming Byerlee's law as describing the weakened state. $\Delta\tau$ shows a strong decrease from about 75% for very low σ_n to 5% to 35% for $\sigma_n \approx 400$ Mpa. Due to the upper bound approximation for τ_s, these values will be *lower* bound approximations for $\Delta\tau$. For $\sigma_n = 0$ $\Delta\tau$ will be equal to 100% for any rock, due to the definition of Byerlee's law.

4.2.2.1. Crustal Scale

A common length scale for modeling processes involving the entire brittle crust, such as formation of orogenic wedges, is $l^* = 2\times10^{-6}$, translating to a model thickness of 5 cm for a brittle crust of 25 km. From equation (2) and assuming $\rho_{\text{model}} = 1700\ \text{kgm}^{-3}$ and $\rho_{\text{nature}} = 2800\ \text{kgm}^{-3}$ this results in a stress scale $\sigma^* = 1.214\times10^{-6}$ (see Table 3). The data from the ring-shear tester are scaled up using this factor, and the rock data are transformed into (τ, σ_n) — space as described above and using the parameters listed in Table 2. The result is shown in Figure 8a.

The peak strength of quartz sand plots in the lower range of the rock failure data and more or less parallel to it. The stable strength of quartz sand plots below and approximately parallel to the curve defined by Byerlee's law. These are both rather good matches, since Byerlee's law marks the upper limit of stable strength. However, for $\sigma_n \leq 200$ MPa the quartz sand data do not follow the kink in Byerlee's law and are thus relatively too high for low normal loads. The strength of glass beads follows the same trend, but since it is generally lower, it does not match the natural data as well as the quartz sand.

As discussed above, the relative weakening $\Delta\tau$ is even more important for the dynamic evolution of a shear zone than the absolute strength, because it can be directly linked to the reactivation potential of a shear zone. $\Delta\tau$ for this scaling is displayed in Figure 8b. It is almost the same for both analog materials, which fully plot in the range of the natural rock data. For very low loads, however, the weakening of rock becomes much larger than that of the analog materials, due to natural rocks' complete loss of strength under these conditions.

Table 3. Scaling Factors for Different Applications of Sandbox Models[a]

Scale	l_{nature} (km)	l_{model} (cm)	$\Delta\rho_{nature}$ (kg m^{-3})	$\Delta\rho_{model}$ (kg m^{-3})	l^*	ρ^*	σ^*
Crust (H)	25	5	1800	1700	2×10^{-6}	0.94	1.89×10^{-6}
Crust (L)	25	5	2800	1700	2×10^{-6}	0.61	1.21×10^{-6}
Basin (H)	10	10	1400	1700	1×10^{-5}	1.21	1.21×10^{-5}
Basin (L)	10	10	2400	1700	1×10^{-5}	0.71	7.08×10^{-6}
Lithosphere (H)	20	1	1800	1700	5×10^{-7}	0.94	4.72×10^{-7}
Lithosphere (L)	20	1	2800	1700	5×10^{-7}	0.61	3.04×10^{-7}

[a](H) = Hydrostatic Pore Fluid Pressure, (L) = Lithostatic Confining Pressure. l thickness of modeled domain, $\Delta\rho$ density reduced by density of pore fluid, and σ stress. g^*, the factor for scaling the acceleration due to gravity, equals 1 in all cases.

4.2.2.2. Other Scales

Sandbox models have been used not only for crustal-scale tectonic models (Table 3) but also to investigate processes on a basin scale (e.g., basin inversion), and granular materials have even been used to represent the entire brittle crust in lithospheric-scale models. Length scales for these cases are on the order of $l^* = 10^{-5}$ and $l^* = 10^{-7}$, respectively. This translates to basin-scale models being about 10 cm thick (for 10 km of sedimentary rock), and the crust in lithospheric-scale models being represented by a 1 cm thick layer of sand (Table 3). For either case Figure 9a shows that the shear strengths of the analog materials are offset with respect to the rock data. For lithospheric-scale models the shear strength of the analog materials is too high, and only the measurements carried out at the lowermost normal load are within the rock data's range of confining pressures. A quantitative comparison is therefore difficult. For the basin-scale case, on the other hand, the analog material's shear strength is too low, the slope of the failure envelopes does not match the natural ones, and the weakening is too small.

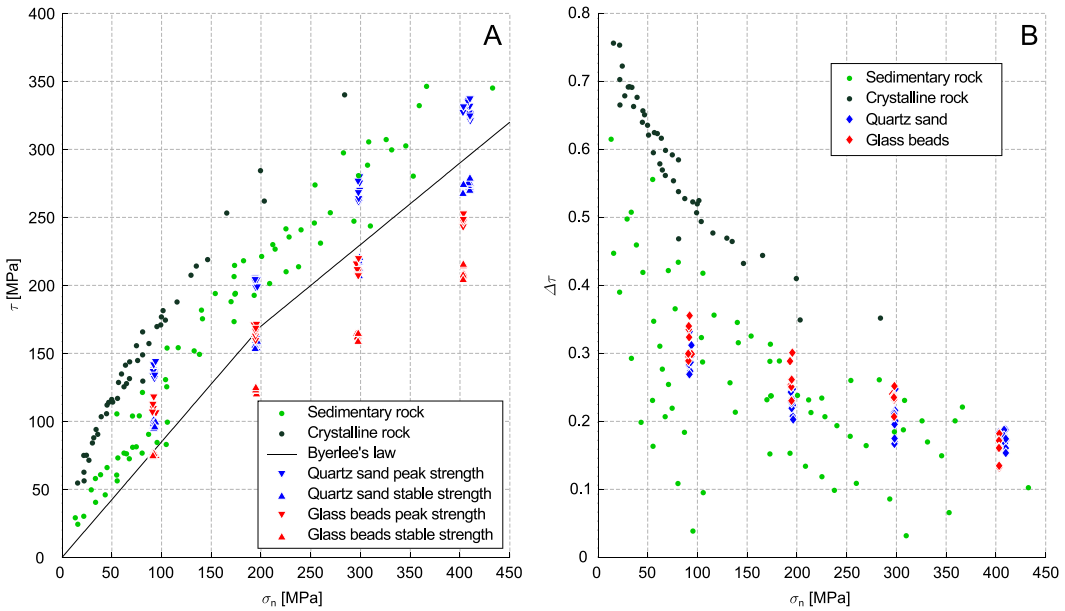

Figure 8. (a) Failure of natural rock and analog materials, scaled for crustal-scale processes and assuming lithostatic stress at depth. The data for the analog materials has been scaled up using a scaling factor of $\sigma^* = \frac{\sigma_{model}}{\sigma_{nature}} = 1.214 \times 10^{-6}$. σ^* has been derived from geometry and density according to equation (2). The rock data have been transformed to (τ, σ_n)—space using friction coefficients from fitted Mohr-Coulomb failure envelopes (original data shown in Figure 7a). Quartz sand matches the natural data rather well, with the peak strength being in the range of natural data and the stable strength somewhat below Byerlee's law [*Byerlee*, 1978], which is an upper bound for natural stable strength. Glass beads are generally too weak to match the natural data. (b) Relative weakening $\Delta\tau$ for rock and analog materials, scaling factor $\sigma^* = \frac{\sigma_{model}}{\sigma_{nature}} = 1.241 \times 10^{-6}$. Both analog materials show very similar $\Delta\tau$ and plot right within the range of natural data.

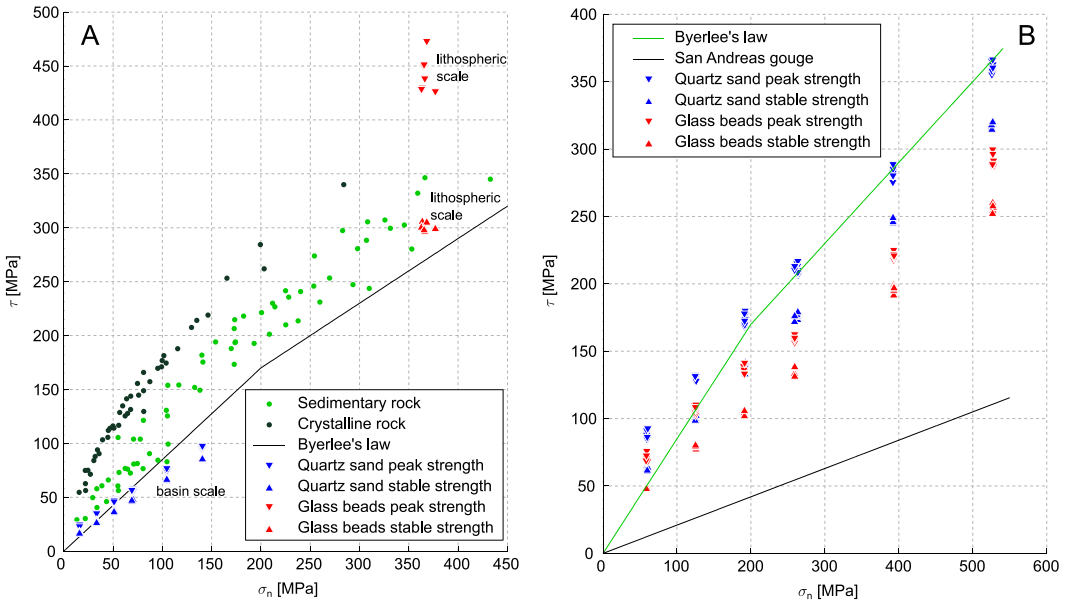

Figure 9. (a) Strength of analog materials for basin- and lithospheric-scale models in comparison to natural rock data. For the lithospheric-scale case the weaker glass beads are shown, for the basin-scale case the stronger quartz sand, but yet the analog materials are to strong respectively too weak in either case. The rock data have been transformed to (τ, σ_n)—space using friction coefficients from fitted Mohr-Coulomb failure envelopes (original data shown in Figure 7). (b) Strength of analog materials scaled to a crust behaving according to Byerlee's law [*Byerlee*, 1978] and under hydrostatic conditions. San Andreas gouge refers to material recovered from drilling the San Andreas Fault, California [*Lockner et al.*, 2011]. Scaling factors in Table 3.

This could potentially be improved by using more cohesive materials, an approach that is, in fact, common in the volcanotectonic community. In Figure 9a this would ideally shift the peak strength upward into the field of natural rock data without affecting the coefficient of internal friction. Table 4 in *Galland et al.* [2015] lists the properties of frequently applied materials, and *Abdelmalak et al.* [2016] present a material of tunable cohesion. However, only peak strengths of the materials are reported, and additional measurements would be required for quantitative comparison.

4.2.2.3. Strain at Failure

An ideally scaled analog material should not only withstand the same (scaled) load as its natural prototype, it should also fail after a similar amount of strain. For the rock data that were digitized from failure curves [*Bieniawski et al.*, 1969; *Crouch*, 1970, 1971] we know this strain threshold to increase slightly with confining pressure and to generally range from 0.2% to 1%, with some measurements reaching up to 4%. These numbers refer to the change of axial sample length normalized to the initial sample length.

To define a similar "bulk axial strain" value for the ring-shear tests, we construct a strain ellipse for each deformation increment during a measurement. We then calculate the length of the short axis of each strain ellipse and call its change in length normalized to its initial length the "axial strain" of these measurements. This yields the following formula for the axial strain in ring-shear tests ϵ_{rst}:

$$\epsilon_{\mathrm{rst}} = 1 - \frac{h}{\sqrt{h^2 + d^2}}. \tag{11}$$

Here h is the height of the shear zone, and d the cumulative displacement at the moment under consideration. However, h cannot be measured during the experiments and therefore needs to be estimated. *Panien et al.* [2006] found the height of a mature shear zone in granular media to be 11 to 16 times the mean grain size, which would correspond to 3.3 mm to 4.8 mm for our quartz sand. *Adam et al.* [2005], on the other hand, observed an approximately 4 cm wide zone of diffuse deformation prior to localization in compressive wedge experiments, using a quartz sand very similar to ours. We assume that this diffuse deformation is also present in our ring-shear experiments at the onset of deformation. Since the maximum possible height of the shear zone in our shear cell (i.e., the height of the shear cell minus the height of the blades at the bottom of the lid) is only 35 mm, we expect the initial shear zone to span the entire shear cell. With progressive deformation

localization will take place and the shear zone will become narrower until it is only 3.3 mm to 4.8 mm wide. Localization and narrowing of the shear zone will be completed shortly after peak stress [*Lohrmann et al.*, 2003], i. e. at peak stress ("failure") the shear zone width will be something between 35 mm and 3.3 mm. This provides a range of possible strain values which lies between 0.03% to 0.11% for 35 mm shear zone width and 3% to 12% for 3.3 mm (quartz sand low-load subset, see displacement data in *Ritter et al.* [2016]). These values are very similar for both quartz sand and glass beads.

Accordingly, rock strain at failure falls within the field of possible values of the analog material's strain at failure. The latter are admittedly still very crude; however, we see no feasible way of deriving more precise values from our data at present.

4.2.3. Comparison to a Fractured Crust

When assuming the crust to be fractured throughout, Byerlee's law (equation (10)) should describe its peak strength. Obtaining values for the weakened strength of crustal faults is difficult, as this is subject of an ongoing debate. Current estimates range from "comparable to the surrounding rock" [*Scholz*, 2000] to friction coefficients as low 0.2 [*Lockner et al.*, 2011]. The latter were measured in shear tests on natural gouge material recovered from drilling the San Andreas Fault, California, whereas the first was estimated from rotation of horizontal stress directions at the same location. We will assume the weakest estimate, keeping in mind that it represents a very mature fault.

Townend and Zoback [2000] showed that in most cases the strength of the brittle crust is not controlled by σ_3, but by the effective stress $\sigma_3 - P_f$, where P_f is the hydrostatic pore fluid pressure. We include this in our scaling by calculating the natural stress as $\sigma_{nature} = (\rho_{crust} - \rho_{fluid})gh$, where ρ_{fluid} is the density of the pore fluid (water). For crustal-scale models ($l^* = 2 \times 10^{-6}$) this leads to a stress scale $\sigma^* = 1.889 \times 10^{-6}$ (Table 3). The scaled strengths are shown in Figure 9b. For $\sigma_n \geq 200$ MPa the upscaled peak strength of quartz sand matches that of the crust nearly perfectly. For lower normal loads it is slightly too high, because it does not follow the kink in Byerlee's law. This kink corresponds to a depth of roughly 7 km in nature or 1.4 cm in crustal-scale model.

The stable strength of quartz sand is much higher than the strength given by the friction coefficient of 0.2 measured for San Andreas gouge. The Glass beads' stable strength is similarly too high; moreover, their peak strength is well below the strength given by Byerlee's law. Since for both analog materials the stable strength is much higher than for the natural example, weakening is too low to properly represent large mature faults.

5. Conclusions

Using a ring-shear tester, we measured frictional properties of two granular materials that are typically applied in analog tectonic modeling. Our results show a change of the frictional properties with normal load, which divides the data into a high-load and a low-load subset. While the high-load subset behaves similar to measurements previously published (weakening through reduction of internal friction) [*Krantz*, 1991; *Lohrmann et al.*, 2003; *Panien et al.*, 2006, the low-load subset shows a behavior that had not been observed so far: weakening through reduction of cohesion. The range of normal loads for which this different frictional behavior is important coincides roughly with the range of normal loads common in analog models, and thus, our findings affects the suitability of these materials for modeling. Importantly, the weakening through reduction of cohesion introduces a scale dependence of material strength, which had previously not been recognized. As a consequence, the tested granular materials are best suited for modeling crustal-scale processes, regardless of whether the actual behavior of the crust is closer to Byerlee's law or laboratory-derived failure envelopes of intact rock. We suggest a length scaling factor of $l^* = 2 \times 10^{-6}$ to obtain the correct dynamically scaled material strength for sandbox models using loose quartz sand. For other length scaling factors the relative weakening and thus the lifetime and reactivation potential of shear zones are likely to be different than in the natural prototype. Glass beads are generally less suited but might be the right choice to model particularly weak structures.

Acknowledgments
M.C.R. and K.L. are funded by the Helmholtz Graduate School GeoSim. The data used in this paper are made available under the following doi: 10.5880/GFZ.4.1.2016.005. The authors thank Kirsten Elger and the GFZ Data Service for publishing the data.

References

Abdelmalak, M., C. Bulois, R. Mourgues, O. Galland, J.-B. Legland, and C. Gruber (2016), Description of new dry granular materials of variable cohesion and friction coefficient: Implications for laboratory modeling of the brittle crust, *Tectonophysics*, *684*, 39–51, doi:10.1016/j.tecto.2016.03.003.

Adam, J., J. Urai, B. Wieneke, O. Oncken, K. Pfeiffer, N. Kukowski, J. Lohrmann, S. Hoth, W. van der Zee, and J. Schmatz (2005), Shear localisation and strain distribution during tectonic faulting new insights from granular-flow experiments and high-resolution optical image correlation techniques, *J. Struct. Geol.*, *27*(2), 283–301, doi:10.1016/j.jsg.2004.08.008.

Al-Ajmi, A. M., and R. W. Zimmerman (2005), Relation between the Mogi and the Coulomb failure criteria, *Int. J. Rock Mech. Min. Sci.*, *42*, 431–439, doi:10.1016/j.ijrmms.2004.11.004.
Bieniawski, Z., H. Denkhaus, and U. Vogler (1969), Failure of fractured rock, *Int. J. Rock Mech. Min. Sci. Geomech. Abstr.*, *6*(3), 323–341, doi:10.1016/0148-9062(69)90009-6.
Brace, W. F., and D. L. Kohlstedt (1980), Limits on lithospheric stress imposed by laboratory experiments, *J. Geophys. Res.*, *85*, B116248, doi:10.1029/JB085iB11p06248.
Brudy, M., M. D. Zoback, K. Fuchs, F. Rummel, and J. Baumgärtner (1997), Estimation of the complete stress tensor to 8 km depth in the KTB scientific drill holes: Implications for crustal strength, *J. Geophys. Res.*, *102*(B8), 18,453–18,475, doi:10.1029/96JB02942.
Brun, J.-P. (1999), Narrow rifts versus wide rifts: Inferences for the mechanics of rifting from laboratory experiments, *Philos. Trans. R. Soc. London, Ser. A*, *357*(1753), 695–712, doi:10.1098/rsta.1999.0349.
Buchanan, P., and K. McClay (1991), Sandbox experiments of inverted listric and planar fault systems, *Tectonophysics*, *188*(1–2), 97–115, doi:10.1016/0040-1951(91)90317-L.
Burchardt, S., and T. R. Walter (2010), Propagation, linkage, and interaction of caldera ring-faults: Comparison between analogue experiments and caldera collapse at Miyakejima, Japan, in 2000, *Bull. Volcanol.*, *72*(3), 297–308, doi:10.1007/s00445-009-0321-7.
Bürgmann, R., and G. Dresen (2008), Rheology of the lower crust and upper mantle: Evidence from rock mechanics, geodesy, and field observations, *Annu. Rev. Earth Planet. Sci.*, *36*(1), 531–567, doi:10.1146/annurev.earth.36.031207.124326.
Byerlee, J. D. (1968), Brittle-ductile transition in rocks, *J. Geophys. Res.*, *73*(14), 4741–4750.
Byerlee, J. D. (1975), The fracture strength and frictional strength of Weber sandstone, *Int. J. Rock Mech. Min. Sci. Geomech. Abstr.*, *12*, 1–4.
Byerlee, J. D. (1978), Friction of rocks, *Pure Appl. Geophys.*, *116*(4), 615–626.
Cobbold, P. R., S. Durand, and R. Mourgues (2001), Sandbox modelling of thrust wedges with fluid-assisted detachments, *Tectonophysics*, *334*(3–4), 245–258, doi:10.1016/S0040-1951(01)00070-1.
Cook, N. (1965), The failure of rock, *Int. J. Rock Mech. Min. Sci. Geomech. Abstr.*, *2*, 389–403, doi:10.1016/0148-9062(65)90004-5.
Crouch, S. L. (1970), Experimental determination of volumetric strains in failed rock, *Int. J. Rock Mech. Min. Sci.*, *7*, 589–603, doi:10.1016/0148-9062(70)90020-3.
Crouch, S. L. (1971), The post-failure behaviour of norite in triaxial compression, *Eng. Geol.*, *6*(6), 19–30, doi:10.1126/science.ns-5.112.260.
Cubas, N., B. Maillot, and C. Barnes (2010), Statistical analysis of an experimental compressional sand wedge, *J. Struct. Geol.*, *32*(6), 818–831, doi:10.1016/j.jsg.2010.05.010.
Cubas, N., C. Barnes, and B. Maillot (2013), Inverse method applied to a sand wedge: Estimation of friction parameters and uncertainty analysis, *J. Struct. Geol.*, *55*, 101–113, doi:10.1016/j.jsg.2013.07.003.
Davy, P., and P. R. Cobbold (1988), Indentation tectonics in nature and experiment. 1. Experiments scaled for gravity, *Bull. Geol. Inst. Uppsala*, *14*, 129–141.
Desrues, J., and G. Viggiani (2004), Strain localization in sand: An overview of the experimental results obtained in Grenoble using stereophotogrammetry, *Int. J. Numer. Anal. Methods Geomech.*, *28*(4), 279–321, doi:10.1002/nag.338.
Dooley, T. P., and G. Schreurs (2012), Analogue modelling of intraplate strike-slip tectonics: A review and new experimental results, *Tectonophysics*, *574–575*, 1–71, doi:10.1016/j.tecto.2012.05.030.
Duerto, L., and K. McClay (2009), The role of syntectonic sedimentation in the evolution of doubly vergent thrust wedges and foreland folds, *Mar. Pet. Geol.*, *26*(7), 1051–1069, doi:10.1016/j.marpetgeo.2008.07.004.
Galland, O., P. R. Cobbold, E. Hallot, J. de Bremond d'Ars, and G. Delavaud (2006), Use of vegetable oil and silica powder for scale modelling of magmatic intrusion in a deforming brittle crust, *Earth Planet. Sci. Lett.*, *243*(3–4), 786–804, doi:10.1016/j.epsl.2006.01.014.
Galland, O., S. Burchardt, E. Hallot, R. Mourgues, and C. Bulois (2014), Dynamics of dikes versus cone sheets in volcanic systems, *J. Geophys. Res. Solid Earth*, *119*(8), 6178–6192, doi:10.1002/2014JB011059.
Galland, O., E. Holohan, B. van Wyk de Vries, and S. Burchardt (2015), Laboratory modelling of volcano plumbing systems: A review, in *Advances in Volcanology*, pp. 1–68, Springer, Berlin, doi:10.1007/11157_2015_9.
Graveleau, F., J. Malavieille, and S. Dominguez (2012), Experimental modelling of orogenic wedges: A review, *Tectonophysics*, *538–540*, 1–66, doi:10.1016/j.tecto.2012.01.027.
Gutscher, M.-A., N. Kukowski, J. Malavieille, and S. E. Lallemand (1996), Cyclical behavior of thrust wedges: Insights from high basal friction sandbox experiments, *Geology*, *24*(2), 135–138, doi:10.1130/0091-7613(1996)024.
Herbert, J. W., M. L. Cooke, P. Souloumiac, E. H. Madden, B. C. Mary, and B. Maillot (2015), The work of fault growth in laboratory sandbox experiments, *Earth Planet. Sci. Lett.*, *432*, 95–102, doi:10.1016/j.epsl.2015.09.046.
Holohan, E. P., T. R. Walter, M. P. Schöpfer, J. J. Walsh, B. van Wyk de Vries, and V. R. Troll (2013), Origins of oblique-slip faulting during caldera subsidence, *J. Geophys. Res. Solid Earth*, *118*(4), 1778–1794, doi:10.1002/jgrb.50057.
Hubbert, M. K. (1937), Theory of scale models as applied to the study of geologic structures, *Bull. Geol. Soc. Am.*, *48*, 1459–1520.
Jaeger, J. C., N. Cook, and R. W. Zimmerman (2007), *Fundamentals of Rock Mechanics*, 4ed., 468 pp., Blackwell Publ., Oxford.
Klinkmüller, M., G. Schreurs, M. Rosenau, and H. Kemnitz (2016a), Properties of granular analogue model materials: A community wide survey, *Tectonophysics*, *684*, 23–38, doi:10.1016/j.tecto.2016.01.017.
Klinkmüller, M., G. Schreurs, and M. Rosenau (2016b), GeoMod2008 materials benchmark: The ring shear test data set, *GFZ Data Serv.*, doi:10.5880/GFZ.4.1.2016.002.
Kolymbas, D., and W. Wu (1990), Recent results of triaxial tests with granular materials, *Powder Technol.*, *60*(2), 99–119, doi:10.1016/0032-5910(90)80136-M.
Krantz, R. W. (1991), Measurements of friction coefficients and cohesion for faulting and fault reactivation in laboratory models using sand and sand mixtures, *Tectonophysics*, *188*(1–2), 203–207, doi:10.1016/0040-1951(91)90323-K.
Leever, K. A., R. H. Gabrielsen, D. Sokoutis, and E. Willingshofer (2011), The effect of convergence angle on the kinematic evolution of strain partitioning in transpressional brittle wedges: Insight from analog modeling and high-resolution digital image analysis, *Tectonics*, *30*(2), doi:10.1029/2010TC002823.
Lockner, D. A., C. Morrow, D. Moore, and S. Hickman (2011), Low strength of deep San Andreas fault gouge from SAFOD core, *Nature*, *472*(7341), 82–85, doi:10.1038/nature09927.
Lohrmann, J., N. Kukowski, J. Adam, and O. Oncken (2003), The impact of analogue material properties on the geometry, kinematics, and dynamics of convergent sand wedges, *J. Struct. Geol.*, *25*(10), 1691–1711, doi:10.1016/S0191-8141(03)00005-1.
Luth, S., E. Willingshofer, D. Sokoutis, and S. Cloetingh (2013), Does subduction polarity changes below the Alps? Inferences from analogue modelling, *Tectonophysics*, *582*, 140–161, doi:10.1016/j.tecto.2012.09.028.
Mandl, G., L. N. J. Jong, and A. Maltha (1977), Shear zones in granular material, *Rock Mech. Felsmech. Mècan. des Roches*, *9*(2-3), 95–144, doi:10.1007/BF01237876.

McClay, K. (1990), Extensional fault systems in sedimentary basins: A review of analogue model studies, *Mar. Pet. Geol.*, *7*(3), 206–233, doi:10.1016/0264-8172(90)90001-W.

Nieuwland, D. A., J. L. Urai, and M. Knoop (2000), In-situ stress measurements in model experiments of tectonic faulting, in *Aspects of Tectonic Faulting*, edited by F. K. Lehner and J. L. Urai, pp. 155–166, Springer, Berlin, doi:10.1007/978-3-642-59617-9_8.

Panien, M., G. Schreurs, and O. A. Pfiffner (2006), Mechanical behaviour of granular materials used in analogue modelling: Insights from grain characterisation, ring-shear tests and analogue experiments, *J. Struct. Geol.*, *28*(9), 1710–1724, doi:10.1016/j.jsg.2006.05.004.

Ritter, M. C., K. Leever, M. Rosenau, and O. Oncken (2016), Supplement to: Scaling the sand box - Mechanical (dis-) similarities of granular materials and brittle rock, *GFZ Data Serv.*, doi:10.5880/GFZ.4.1.2016.005.

Rosenau, M., J. Lohrmann, and O. Oncken (2009), Shocks in a box: An analogue model of subduction earthquake cycles with application to seismotectonic forearc evolution, *J. Geophys. Res.*, *114*, B01409, doi:10.1029/2008JB005665.

Schellart, W. (2000), Shear test results for cohesion and friction coefficients for different granular materials: Scaling implications for their usage in analogue modelling, *Tectonophysics*, *324*(1–2), 1–16, doi:10.1016/S0040-1951(00)00111-6.

Scholz, C. H. (2000), Evidence for a strong San Andreas fault, *Geology*, *28*, 163–166, doi:10.1130/0091-7613(2000)28<163:EFASSA>2.0.CO;2.

Scholz, C. H. (2002), *The Mechanics of Earthquakes and Faulting*, 2nd ed., 471 pp., Cambridge Univ. Press, Cambridge.

Schulze, D. (1994), Development and application of a Novel Ring Shear Tester, *Aufbereitungstechnik*, *35*(10), 524–535.

Townend, J., and M. D. Zoback (2000), How faulting keeps the crust strong, *Geology*, *28*(5), 399–402, doi:10.1130/0091-7613(2000)28<399:HFKTCS>2.0.CO.

Tron, V., and J.-P. Brun (1991), Experiments on oblique rifting in brittle-ductile systems, *Tectonophysics*, *188*(1–2), 71–84, doi:10.1016/0040-1951(91)90315-J.

van Mechelen, J. (2004), Strength of moist sand controlled by surface tension for tectonic analogue modelling, *Tectonophysics*, *384*(1–4), 275–284, doi:10.1016/j.tecto.2004.04.003.

Wawersik, W. R., and C. Fairhurst (1970), A study of brittle rock fracture in laboratory compression experiments, *Int. J. Rock Mech. Min. Sci. Geomech. Abstr.*, *7*, 561–575, doi:10.1016/0148-9062(70)90007-0.

Weijermars, R., and H. Schmeling (1986), Scaling of Newtonian and non-Newtonian fluid dynamics without inertia for quantitative modelling of rock flow due to gravity (including the concept of rheological similarity), *Phys. Earth Planet. Inter.*, *43*(4), 316–330, doi:10.1016/0031-9201(86)90021-X.